INTERNATIONAL JOURNAL OF OPTIMIZATION IN CIVIL ENGINEERING
Int. J. Optim. Civil Eng., 2024; 14(1):37-60

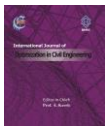

OPTIMIZING SEISMIC PARAMETERS OF DESIGN LATERAL FORCE PATTERN IN PERFORMANCE-BASED PLASTIC DESIGN OF SMR FRAMES WITH GENETIC PROGRAMMING

A. Hadinejad[1,2] and B. Ganjavi[1*, †]
[1] *Department of Civil Engineering, University of Mazandaran, Babolsar, Iran*
[2] *School of Civil Engineering, Collage of Engineering, University of Tehran, Tehran, Iran*

[DOI: 10.22068/ijoce.2024.14.1.574]

ABSTRACT

In this study, the investigation of maximum inelastic displacement demands in steel moment-resisting (SMR) frames designed using the Performance-Based Plastic Design (PBPD) method is conducted under both near-fault and far-fault earthquake records. The PBPD method utilizes a target drift and predetermined yield mechanism as the functional limit state. To accomplish this, 6 steel moment frames having various heights were scaled using well-known $sa(T_1)$ method and, then, were analyzed by OPENSEES software. A total of 22 far-fault records and 90 near-fault records were compiled and employed for parametric nonlinear dynamic analysis. The near-fault records were classified into two categories: $T_1/T_p \geq 1$ and $T_1/T_p < 1$. The study aimed at investigate their impacts on the inter-story drift and the relative distribution of base shear along the height of the structure. The results revealed that the records with $T_1/T_p \geq 1$ exerted the greatest influence on the drift demands of upper stories in all frames. Conversely, the near-fault records with $T_1/T_p < 1$ demonstrated the most significant impact on the lower stories of mid-rise frames. Additionally, the distribution of relative story shears was examined through genetic programming for optimum PBPD design of steel moment frame structures. As a result, a proposed relationship, denoted as b (seismic parameter for design lateral force distribution), was developed and optimized for both near-fault and far-fault records. This relationship depends on the fundamental period of vibration and the total height of the structure. The accuracy of the predicted model was assessed using R^2, which confirmed the reliability of the proposed relationship.

Keywords: Performance-Based Plastic Design (PBPD), Genetic Programming, Optimization, Seismic Parameter for Design Lateral Force Distribution.

Received: 6 November 2023; Accepted: 27 December 2023

[*]Corresponding author: Department of Civil Engineering, University of Mazandaran, Babolsar, Iran
[†]E-mail address: b.ganjavi@umz.ac.ir (B. Ganjavi)

1. INTRODUCTION

The conventional approach to structural design involves a force-based method, which includes estimating gravity and lateral forces, distributing them vertically, and determining the required strength of structural components. In this method, shear forces are typically obtained assuming elastic behavior, and the correction for inelastic response is made through behavior factors. However, performance-based design methods have gained popularity in recent years due to their ability to determine a structure's response to specific performance goals. Structural engineers are increasingly adopting these methods for designing new buildings.

Performance-based plastic design (PBPD) is a relatively new seismic design method which is basically derived from conventional performance-based design approaches. PBPD, introduced by Goel et al. [1–3], is a direct design method that eliminates the need for post-design evaluation. It considers the balance of work and energy, displacement of structural elements, and predicted yield mechanisms to calculate the required foundation strength. Unlike traditional trial-and-error-based methods, PBPD incorporates nonlinear functional parameters and required plasticity during the design process, eliminating the necessity for iterative design iterations. Furthermore, PBPD allows for multiple performance goals to address various risk levels associated with earthquakes. Numerous researchers have investigated the application of PBPD to different types of steel structures. They have developed PBPD approaches specifically to these structures, aiming at calculate base shear design based on energy work theory for elasto-plastic equivalent single-degree-of-freedom (SDOF)systems. One important parameter in PBPD is the coefficient *b*, which is required to determine shear and distribute lateral forces. Goel introduced this coefficient for steel moment frame structures based on the analysis of 2-20 story structures and the averaging of their responses [2].

Many studies have extensively investigated the application of Performance-Based Plastic Design (PBPD) for various 2D structural systems. Bayat [4] developed the PBPD approach specifically for concentrically braced frames, tall moment frames, and plate shear wall frames. Liao [5] and Liao and Goel [6], utilized the PBPD method to design reinforced concrete moment frames. The PBPD method has also been extended to other structural systems, including dual moment and eccentrically-braced frames [7], the eccentrically braced frames with vertical link [8], special truss moment frames [9], buckling-restrained braced frames [10], tall hybrid coupled walls [11], and dual moment frames with steel plate shear wall systems [12], the dual buckling-restrained braced reinforced concrete moment frames [13]. Researchers have been trying to understand the behavior of PBPD frames combined with other structural concepts such as soil-structure interaction [14,15],structural control [16] and mainshock-aftershock sequence [17]. The effectiveness and applicability of the proposed PBPD technique for different types of self-centering (SC) structures, including low-rise and high-rise special moment-resisting frames (SMABFs), were investigated by Qiu et al. [18]. The results demonstrated that the structures exhibited no residual deformation and returned to their original resting state. Hou et al. [19] further expanded on this by creating three 6-story SMABFs using three different types of shape memory alloys (SMAs) with varying hysteretic behavior. They have discovered that the energy modification factor in structural control structures depends not only on the ductility factor (μ) and natural period (T) but also on the

[DOI: 10.22068/ijoce.2024.14.1.574]

hysteretic characteristics. Furthermore, by employing a lateral load distribution pattern with a period coefficient of 0.75, researchers were able to reduce the effects of higher-modes in structural responses. In addition to investigating evaluation of the behavior of PBPD frames under scaling of near-fault and far-fault records [20], researchers have made significant efforts to understand the performance of PBPD frames. These findings indicate that PBPD theories can be modified to accommodate various structural materials by adjusting a few key parameters. Newmark and Hall [21], and Lee [2] have proposed modifying ductility reduction and energy modification factors for specific structural systems.

Nowadays, the use of advanced mathematical methods and computational techniques has opened up new possibilities for accurate calculations of the coefficient *b*. One of them is genetic programming (GP), which is a branch of genetic algorithms. GP was initially proposed by Koza [22], who outlined a four-step process for its implementation. The first step involves creating an initial population of equations by randomly combining problem-specific functions and terminals. The correctness of each equation generated in the previous step is then evaluated. In the next phase, a new population is generated using genetic operators and selecting the best equations from the current population. If the desired number of generations has been reached, the optimal equation is identified in the fourth phase; otherwise, the process continues from the second step. The primary objective of GP is to find an equation within the solution space that most accurately represents the desired response. The GP process involves a blind and random search for an appropriate equation, and it is crucial to minimize the size of the equation trees to avoid the generation of lengthy and redundant equations.GP draws inspiration from machine learning techniques and applies them to evolve computer programs that can perform specific tasks. It begins by creating a random population of computers, typically structured as trees, and then selects the best-performing programs to form a new population. This iterative process continues until the population consists of programs that satisfactorily solve the given problem [23–25]. In the context of symbolic data mining (SDM), empirical mathematical models are created based on data collected from a system or process. SDM encompasses various tasks, such as symbolic regression (developing symbolic equations to predict continuous-valued response variables using input/predictor variables), extended classification (predicting the discrete category of a response variable using input variables), and symbolic optimization (creating equations to optimize other criteria). Numerous studies have been conducted to enhance forecast accuracy and develop reliable models using a variety of techniques. In previous studies, various data mining techniques have been successfully applied in different engineering and technology domains to make accurate predictions. Kaveh [24] demonstrated the effectiveness of artificial neural network (ANN) models in forecasting the compressive strength of concrete, showing their ability to predict values. Baykasoglu [26] utilized genetic programming (GP) to forecast the strength of limestone at greater depths, using input variables such as water absorption, ultrasonic pulse velocity, dry density, saturation density, and bulk density. The study conducted by Savic et al. [27] showcased the potential of GP in runoff output modeling, employing rainfall and evaporation data as input variables [28,29]. Additionally, researchers have widely employed data mining techniques in various engineering and technology domains, providing substantial evidence of their ability to make accurate predictions [27, 30–33].

The main goal of this study is to parametrically investigate the influence of 22 far-fault

[DOI: 10.22068/ijoce.2024.14.1.574]

records and large numbers of 90 near-field records, scaled using the first mode period method ($sa(T_1)$), on the nonlinear response of steel moment frames designed based on PBPD method. Furthermore, the near-fault records are categorized into two groups: $T_1/T_p \geq 1$ and $T_1/T_p < 1$. Also, previous research studies have not adequately addressed the impact of near-fault earthquakes and the modification of the coefficient b in the PBPD method, which has traditionally been solely dependent on the structure's period parameter. Therefore, this study seeks to establish a suitable relationship for optimum b value using genetic programming (GP) for both far- fault and near-fault earthquakes, while also examining its dependence on the height of the structure. To this end, eight steel moment frames with different number of stories of 4, 6, 8, 10, 12, 14 and 16 were designed using the PBPD method under the target Design-Based Earthquake (DBE) spectrum. These structures were then analyzed to evaluate the effects of near and far records on the distribution of required displacements and the relative shear distributions. Additionally, through an optimization algorithm using GP method the optimal coefficients of b have been proposed. The data used in this study were obtained from the analysis of these structures using OpenSees software and were divided into two groups:

1. Training data set: This set was utilized to develop the model based on the provided information.
2. Testing data set: This set was employed to assess the effectiveness and accuracy of the model.

By utilizing these data sets, the study aims to assess the performance of the PBPD method and the precision of the calculated coefficient b in predicting the nonlinear response of steel moment frames subjected to both far-fault and near-fault earthquake ground motions.

2. DETAILS OF PBPD AND GENETIC PROGRAMMING

2.1. Energy equilibrium equation

The majority of construction regulations make the inaccurate premise that structural nonlinearity may only alter the amplitude of structural reactions and not the distribution of shear forces over height [1]. The equations for the energy equilibrium are presented as follows [34]:

$$E_i = E_k + E_\xi + E_a \tag{1}$$

$$E_a = E_s + E_h \tag{2}$$

where E_k, E_ξ, E_a, E_i, E_s and E_h are kinetic, damping, absorbed, earthquake input, elastic strain and irrecoverable hysteretic energy, respectively. After an earthquake, the kinetic energy and elastic strain energy are no longer present [35]. The input energy is attenuated by the damping energy and the energy absorbed within the structure, particularly when the ductility factor exceeds 2. It is worth noting that there is a slight distinction between the irrecoverable hysteretic energy and the absorbed energy [36]. In a nonlinear system, the damping energy has a smaller influence compared to the absorbed energy in attenuating the

[DOI: 10.22068/ijoce.2024.14.1.574]

input energy [35]. Consequently, the energy equilibrium equation for a nonlinear system can be expressed as follows [1]:

$$E_i = E_s + E_h \tag{3}$$

Many researchers have attempted to compute the above equation's terms. for elastic behavior, Housner [37] presented the following formula for a SDOF system's input energy:

$$E_i = \frac{1}{2} M S_v^2 \tag{4}$$

where M and S_v represent for, respectively, seismic mass and spectral response velocity. When T, the structure's period, is shorter than 3 s, the aforementioned equation seems to be true. Lee [2] introduced an energy modification factor that made the formula more generic and applicable to periods outside the original range:

$$E_i = \gamma\left(\frac{1}{2} M S_v^2\right) \tag{5}$$

$$\gamma = \frac{2\mu_s - 1}{R_\mu^2} \tag{6}$$

where R_μ is the ductility reduction factor suggested by Newmark and Hall [21] and μ_s is the structural ductility factor. The following formula was suggested by Akiyama [38] for calculating elastic strain energy:

$$E_i = \frac{1}{2} M S_v^2 \tag{7}$$

where V and W represent for the seismic weight and base shear, respectively.

2.2. Performance-based plastic design method

The PBPD approach was introduced as an energy-based design method by Goel et al. [39]. They applied Lee's [2] nonlinear base shear distribution over height. The α coefficient in Equations (8) and (9) was modified to 0.75 by Chao et al. [40] and Chao and Goel [40].

$$\beta_i = \left(\frac{\sum_{j=i}^{n} w_j h_j}{w_n h_n}\right)^{\alpha T^{-0.2}} \tag{8}$$

$$\lambda_i = (\beta_i - \beta_{i+1})\left(w_n h_n \Big/ \sum_{j=i}^{n} w_j h_j\right)^{\alpha T^{-0.2}} \quad \text{and} \quad F_i = \lambda_i V \tag{9}$$

[DOI: 10.22068/ijoce.2024.14.1.574]

where i is the story number and, respectively, w, h, and F stand for the seismic mass, story height, distribution coefficient, and lateral force associated with story number i. n is the number of stories and V is the total base shear in the equation above. The energy equilibrium equation of the PBPD-2D technique [9] is finally expressed as Eq. (10), which calculates the hysteretic energy based on a pre-selected yield mechanism as illustrated in Fig. 1 and uses the Eqs. (3) to (7).

$$\frac{1}{2}\left(\frac{W}{g}\right)\times\left(\frac{T}{2\pi}\times\frac{V_y}{W}g\right)^2+V_y\left(\sum_{i=1}^{n}\lambda_i h_i\right)\theta_p=\frac{1}{2}\gamma\left(\frac{W}{g}\right)\times\left(\frac{T}{2\pi}\mathrm{S_a}g\right)^2 \tag{10}$$

where V_y is the yield base shear in Eq. (10), p is the structure's plastic rotation as indicated in Fig. 1, and other factors were already covered in the sections above. To mitigate the soft-story mechanism, the plastic moment of the first-story columns is determined. In accordance with Eq. (11), this moment is augmented by a coefficient that accounts for the impact of the design resistance factor for beams, yield over strength factor for beams, strain hardening of beams, and over size factor [41].

$$M_{pc}=\frac{1.5Vh_1}{4} \tag{11}$$

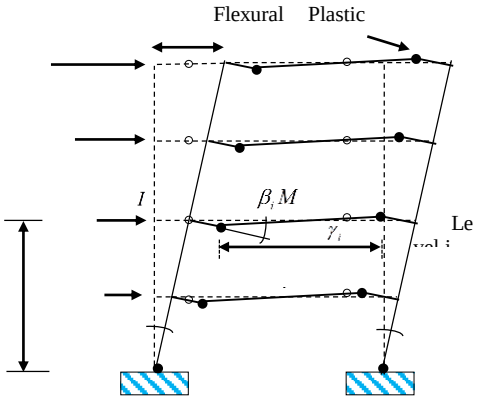

Figure 1. Single-bay frame prototype with predefined mechanism and plastic hinges in beams and columns end

where h_1 is the height of the first story and V is the bay's share of the frame's overall base shear.

When calculating the yield base shear of a multi-bay frame, the total base shear is divided by the number of bays to get the fraction of the base shear for a bay. As a result, constructing a frame with multiple equal bays is switched to creating multiple identical one-bay frames. For the one bay frame shown below [3], the internal and exterior work are equalized to yield the

[DOI: 10.22068/ijoce.2024.14.1.574]

moment of the beams:

$$\sum_{i=1}^{n} F_i h_i \theta_p = 2M_{pc}\theta_p + \sum_{i=1}^{n} 2(\beta_i M_{pb})\gamma_i \quad (12)$$

And the column tree approach is used to create the columns [4, 9]. The plastic rotation of beams is likely bigger than the plastic rotation of the frame [39] (θ_p). Since a concentrate model is used to represent the plastic hinges, the rising coefficient is equal to the ratio of the distance between the plastic hinges and the beam as shown below:

$$\gamma = \frac{L}{L'}\theta_p \quad (13)$$

where L and L', as illustrated in Fig. 1, are the beam's length and the separation between its two plastic hinges, respectively.

3. DETAILS OF STRUCTURES AND EARTHQUAKES

3.1. Details of Frames

To accomplish the research objectives, a set of frames consisting of different numbers of floors was utilized. Specifically, frames with 4, 6, 8, 10, 12, 14, 16, and 18-stories were considered. The period of the first mode and other relevant specifications for these frames are provided in Table 1. It is worth noting that the frames were initially modeled using OpenSees software [42] and subsequently analyzed using MATLAB software to obtain the desired results.

The characteristics of the beams and columns of steel moment frames designed using the PBPD method are illustrated in Fig. 2.

Table 1. Design parameters of frames, target displacement of 2%

Story	T(S)	C_e	yield drift	θ_p	α	γ	V/W
4	0.75	0.94	0.01	0.01	2.04	0.75	0.283
6	0.98	0.76	0.01	0.01	1.62	0.75	0.236
8	1.26	0.66	0.01	0.01	1.38	0.75	0.207
10	1.46	0.59	0.01	0.01	1.24	0.75	0.185
12	1.66	0.54	0.01	0.01	1.13	0.75	0.169
14	1.88	0.50	0.01	0.01	1.04	0.75	0.157
16	2.14	0.47	0.01	0.01	0.97	0.75	0.146
18	2.34	0.44	0.01	0.01	0.88	0.75	0.138

[DOI: 10.22068/ijoce.2024.14.1.574]

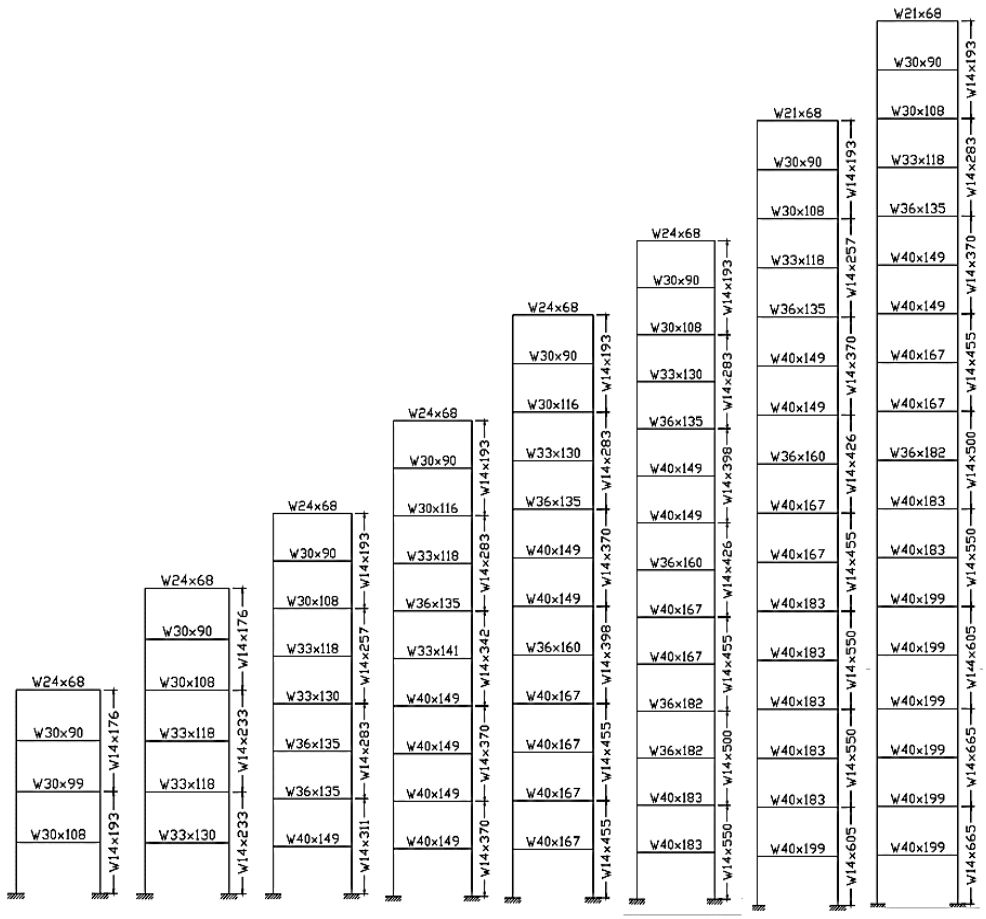

Figure 2. Selected 4-, 6-, 8-, 10-, 12-, 14-, 16-, 18-story moment frames

3.2. Selection of near-fault records

The earthquake pulse period near a fault is a critical parameter when studying the response of multi-degree-of-freedom (MDOF) structures to such earthquakes. These pulse-type earthquakes can lead to a non-uniform distribution of floor ductility requirements in code-compliant structures, significantly impacting the expected code levels. In this study, the chosen method for analyzing earthquakes near-fault is based on the ratio of the structure's main period to the earthquake pulse period (d).According to the research conducted by Alavi and Krawinkler [43], the behavior of multi-story frames is strongly influenced by the comparison between the main period of the system and the pulse period. For instance, structures designed based on shear strength using the square root method, SRSS, are expected to have higher maximum ductility requirements at the bottom of the frame, regardless of the overall structural strength. Conversely, in strong structures, if the main period is longer (D), the maximum ductility demand is anticipated to occur at the top of the frame, while weaker structures experience greater ductility demands at the bottom.

The selection of near-fault earthquakes for this study is based on the research conducted by Baker et al. in 2011 [44]. This study includes 90 near-fault pulse-type earthquakes with a

[DOI: 10.22068/ijoce.2024.14.1.574]

wide range of pulse periods and characteristics of C and D soils [45]. These earthquakes are classified based on the studies of Park and Medina [48] within the $0.35 < T_1/T_p \leq 3.0$ range. The records have a magnitude of $6 \leq M_w \leq 7.9$, and located at a distance of less than 20 km from the fault, and have a maximum ground velocity (PGV) greater than 20 cm/s. It is important to note that all pulse-type earthquakes in this study have been rotated 90 degrees in the direction of the fault using the MATLAB program. For the analysis, only the components perpendicular to the fault have been considered. The list of near-fault earthquakes can be found in Table 3, which is available in reference [20]. Structures designed based on the PBPD method are divided into two groups: near-fault records with $T_1/T_p \geq 1$ and near-fault records with $T_1/T_p < 1$. The number of records in each group, based on the structure's period, is provided in Table 2.

Table 2. Number of near-fault ground motions for each frame

$0.35 < T_1/T_p \leq 3.0$			
Story	T_1	$T_1/T_p < 1$	$T_1/T_p \geq 1$
4	0.75	29	3
6	0.98	32	6
8	1.26	31	17
10	1.46	30	21
12	1.66	31	24
14	1.88	33	28
16	2.14	32	30
18	2.34	34	33

3.3. Selection of far-fault records

In this study, earthquake records located more than approximately 13 km away from the rupture zone and without pulse-type features were utilized. For comparison purposes, 22 representative earthquakes were selected, characterized by a distance of $13km \leq R_r \leq 40km$ and magnitudes $6 \leq M_w \leq 7$ and $PGV \geq 20cm/s$, specifically for soil type D (NEHRP Site Class D) [45]. The analysis focused on the strong component of each earthquake. The list of selected earthquakes can be found in Table 4, which is available in reference [20].

3.4. Target Spectrum

To utilize any of the proposed methods for scaling ground motion and conducting dynamic analysis of structures, one of the necessary parameters is the spectral acceleration values corresponding to specific target periods. These values are calculated based on a desired spectrum. For this study, the objective is to extract the desired spectra for the Riverside area of California (Riverside-Latitude=33.982°N, Longitude=117.374°W). This can be achieved using the USGS website [46] and selecting the spectral design for the design basis earthquake (DBE) at a risk level of 10% in 50 years (2/3MCE).

All the earthquake records are then scaled to match the period of the first mode of the structure. An example of the scaled records can be seen in Fig. 3, illustrating the relationship

[DOI: 10.22068/ijoce.2024.14.1.574]

between the spectral acceleration values and the corresponding periods. This scaling process ensures that the ground motion data aligns with the structural characteristics and allows for accurate dynamic analysis of the structures under consideration.

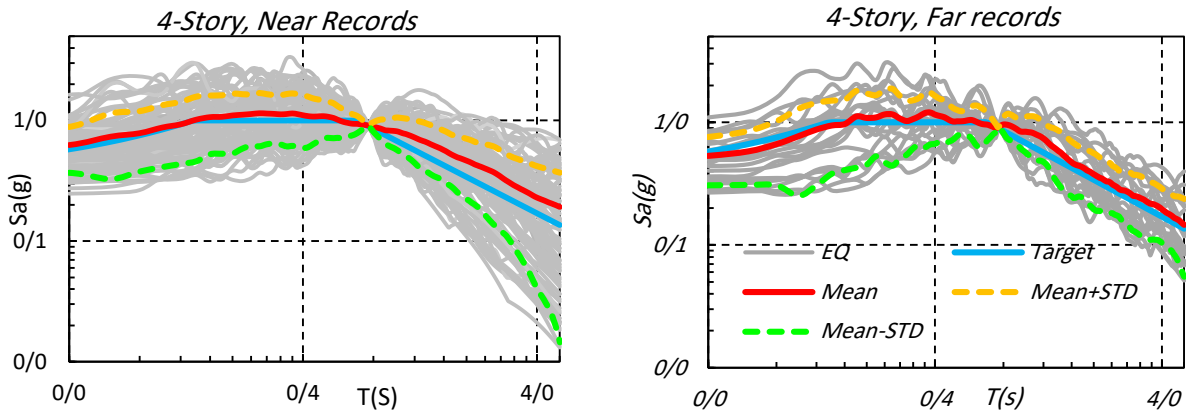

Figure 3. Comparison of scaled records using $Sa(T_1)$for 4-story, far and near fault

4. GENERAL ANALYSIS PROCEDURE AND METHODOLOGY

The general analysis process of this study can be divided into three sections: In the first section, we analyze the maximum drift distribution over height of the structures in three categories of earthquake records: far-fault, near-fault with $T_1/T_p \geq 1$, and near-fault with $T_1/T_p < 1$. Then, the results obtained from these categories will be examined and compared to assess their impact on the structural response. This analysis aims to understand how different earthquake scenarios affect the maximum drift of the structures. Moving on to the second section, this paper investigates the values of V_i/V_n, which represent the ratio of the relative shear distributions, for those earthquake records. This assessment can evaluate the structural performance under various seismic events. By examining this ratio, we can gain valuable insights into the adequacy of the structures to withstand different levels of ground motion. In the final section, The genetic programming was utilized to optimize the relationship parameter "b" in the design of steel moment frame structures using the PBPD method. The objective is to optimize the value of "b" by utilizing the genetic programming which will be described in the upcoming section, considering desired performance criteria and structural requirements. This optimization process leads to a refined relationship that enhances the accuracy and efficiency of the design process for steel moment frame structures using the PBPD method. The proposed relationship can then be presented and applied in the design of such structures.

The GPTIPS toolbox, developed by Searson at Newcastle University [23, 25], is a powerful tool for applying genetic programming techniques to discover equations that solve specific problems. It aids in the exploration and optimization of equations using GP techniques, particularly through symbolic regression, which enables the identification of mathematical formulas capable of predicting or explaining a given dataset. Symbolic regression automates

[DOI: 10.22068/ijoce.2024.14.1.574]

the process of creating equation structures and estimating their values, allowing for the discovery of equations with inputs and the capture of non-linear phenomena. These symbolic regression models typically consist of an output variable (y) to be predicted, a model prediction (ŷ), input or predictor variables (x_1,...,x_2), and a symbolic non-linear function (f). GPTIPS employs multigene genetic programming (MGGP), a variant of genetic programming, to generate and improve equations by evolving data structures encompassing multiple trees or genes. This versatile genetic programming platform is designed with a pluggable architecture, enabling users to easily integrate their own objective/fitness functions for tasks like symbolic classification and optimization into GPTIPS without modifying its core code. The specialized features of GPTIPS tailored for developing multigene symbolic regression models leverage the advantages of MGGP, allowing the evolution of new equation model terms and their optimal combination using linear least squares parameter estimation. Extensive research has demonstrated the effectiveness of multigene symbolic regression in evolving accurate and compact models, even with a large number of input variables exceeding 1500, making it more efficient than traditional GP approaches for modeling nonlinear problems [28], [29].

5. RESULTS AND DISCUSSIONS

5.1. Height-wise distribution of maximum inter-story drift

Fig. 4 presents the response of eight structures to far-fault earthquake records. In shorter structures, the maximum drift always occurs in the lower stories when subjected to far-fault records. However, as the height of the structure increases, the drift progressively amplifies in the upper stories. It is noteworthy that although the average drift of the records also increases with the structure's height, it consistently remains below the target drift in all cases. This observation demonstrates the effectiveness of the structural design in meeting the target drift and ensuring the fulfillment of performance objectives.

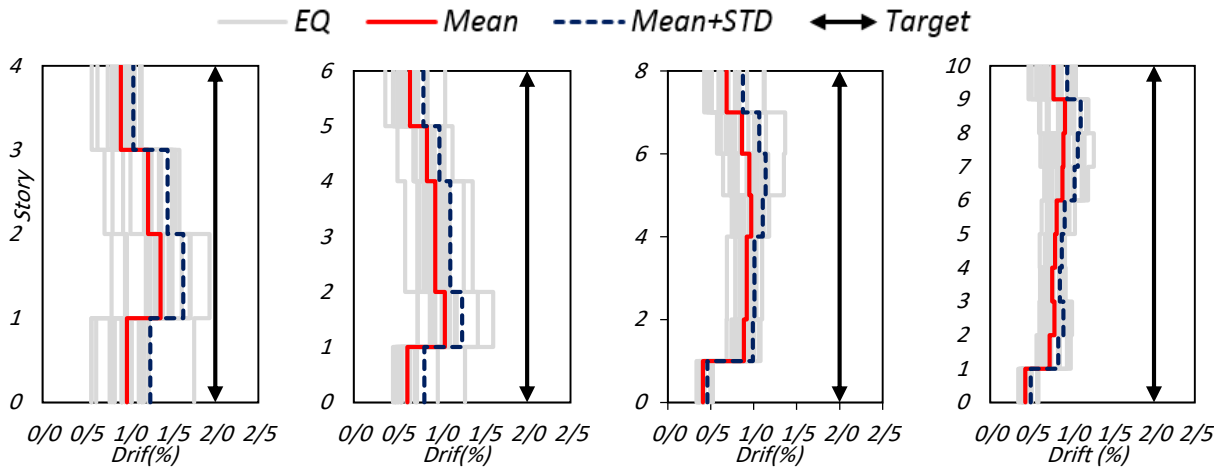

[DOI: 10.22068/ijoce.2024.14.1.574]

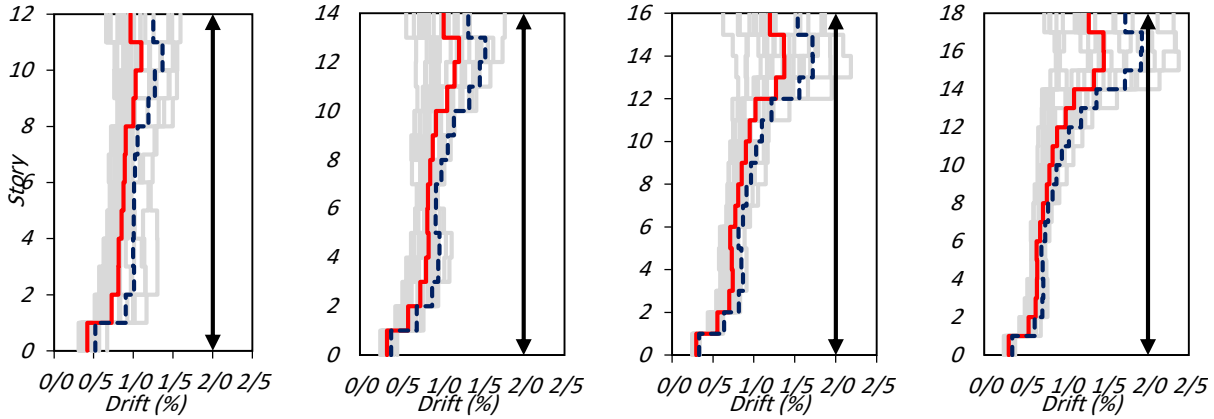

Figure 4. Distribution of mean and mean + STD drifts over the height of structures subjected to far-fault records

Moving on to Fig. 5, it exhibits the maximum drift values of the structures when subjected to near-fault records with $T_1/T_p \geq 1$, where T_1 represents the fundamental period of the record and T_p represents the pulse period. Notably, even in structures with relatively lower heights, the upper stories exhibit the highest average drift. This phenomenon can be attributed to the presence of a pulse period resulting from the near-fault records included in this specific group. The near-fault records in this group possess distinctive characteristics, including their proximity to the structure and unique ground motion properties. These factors contribute to a pulse-type response, where the upper stories experience higher drift values compared to the lower stories. The influence of the pulse period, a characteristic feature of these near-fault records, significantly impacts the distribution of drift within the structure. This observation emphasizes the importance of considering the specific characteristics of near-fault records, particularly for structures located in close proximity to seismic sources.

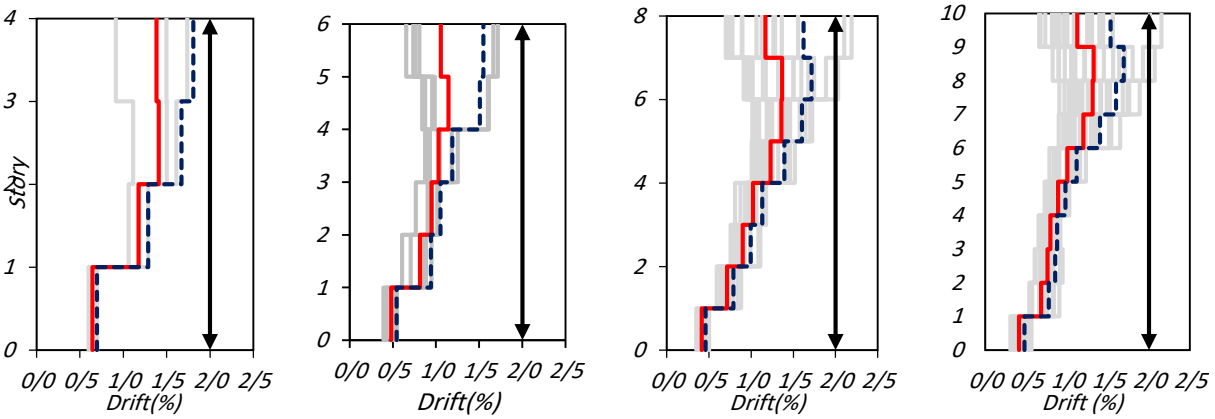

[DOI: 10.22068/ijoce.2024.14.1.574]

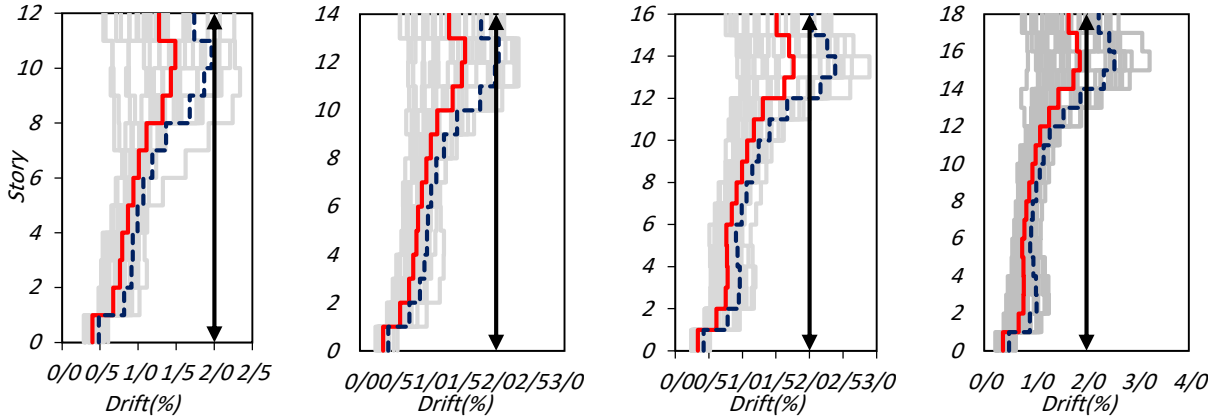

Figure 5. Distribution of mean and mean + STD drifts over the height of structures subjected to near-fault records with $T_1/T_p \geq 1$

For the second part of the aforementioned periodic ratio, Fig. 6 is provided to focus on the evaluation of structures under near-fault records with $T_1/T_p < 1$. The findings reveal that these records lead to an increase in the average drift in the middle stories of short to mid-rise structures. However, as the height of the structure exceeds 14 stories, a noticeable escalation in drift is observed in the upper stories. The observed trend emphasizes the distinct effect of near-fault records with $T_1/T_p < 1$ on the structural response. In shorter to mid-rise structures, the middle stories bear the primary impact of the increased drift due to the influence of these records. As the structure's height surpasses, 14 stories, the near source records begin to exert a more pronounced effect on the upper floors, resulting in an elevated drift in those levels. These findings highlight the significance of considering the specific characteristics of near-fault pulse-type records, particularly when $T_1/T_p < 1$, during the design and assessment of structures. Adequate attention should be given to understanding the response behavior of the middle and upper floors to ensure overall structural integrity and performance under such seismic scenarios.

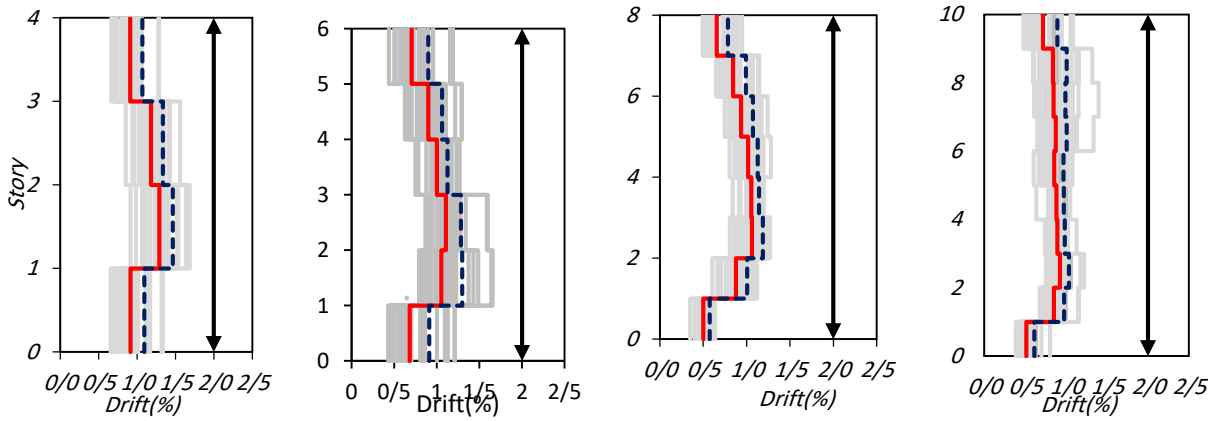

[DOI: 10.22068/ijoce.2024.14.1.574]

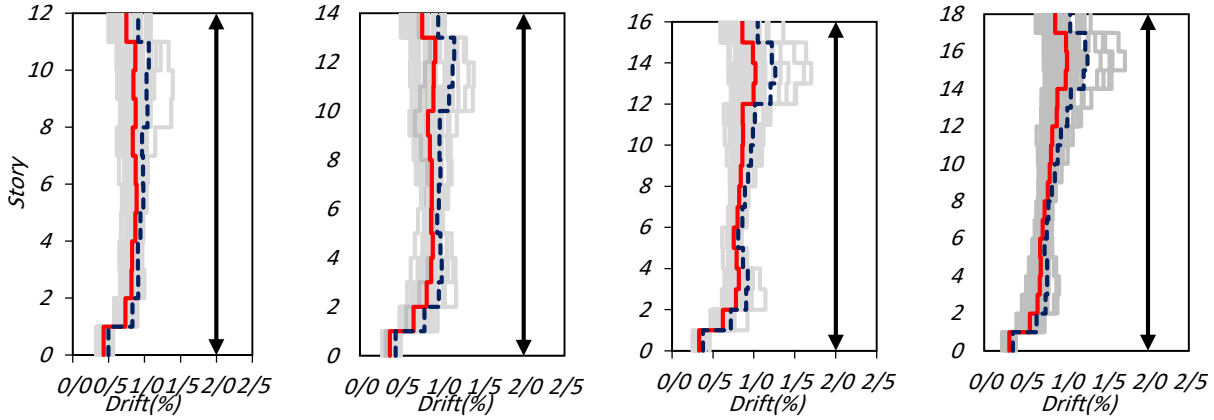

Figure. 6 Distribution of mean and mean + STD drifts over the height of structures subjected to near-fault records with $T_1/T_p < 1$

The maximum drifts of frames ranging from 4 to 18 stories are compared across three record categories, including far-fault, near-fault with $T_1/T_p \geq 1$, and near-fault with $T_1/T_p < 1$, in Figure 7. It can be observed that in shorter structures with 4 and 6 stories, the maximum drift of the $T_1/T_p < 1$ records category is respectively 6.6% and 10% higher than the maximum drift of the far-fault records category. However, as the frame height increases in structures with 8 and 10 stories, the $T_1/T_p < 1$ records category experiences the highest amount of drift in the lower floors, with the difference reaching 22.8% and 20.1% for these two frames, respectively. For frames with 12, 14, 16, and 18 stories, there is still a higher maximum drift (3.1%, 11.7%, 12.2%, and 6.6%, respectively) in the $T_1/T_p < 1$ records category compared to the far-fault records in the lower stories. This demonstrates that the $T_1/T_p < 1$ records, due to their specific frequency content, have the greatest effect on the drift of the lower stories in the mid-rise 8- and 10-story structures, requiring more displacement. Moreover, when examining the maximum drift of $T_1/T_p \geq 1$ records compared to far-fault records, it is evident that the maximum drift of $T_1/T_p \geq 1$ records is highest in the upper stories of all frames, ranging from 28.4% to 71.1% across various structures. This indicates that the upper stories are more affected by the $T_1/T_p \geq 1$ records. Finally, in the 18-story structure, the maximum drift value of $T_1/T_p \geq 1$ records is very close to the target drift (2%).

In summary, the comparison of these records highlights the significant effects of $T_1/T_p < 1$ records on the drift of the lower stories in the mid-rise 8- and 10-story structures, while the far-fault records and $T_1/T_p \geq 1$ records have a stronger influence on the upper stories.

[DOI: 10.22068/ijoce.2024.14.1.574]

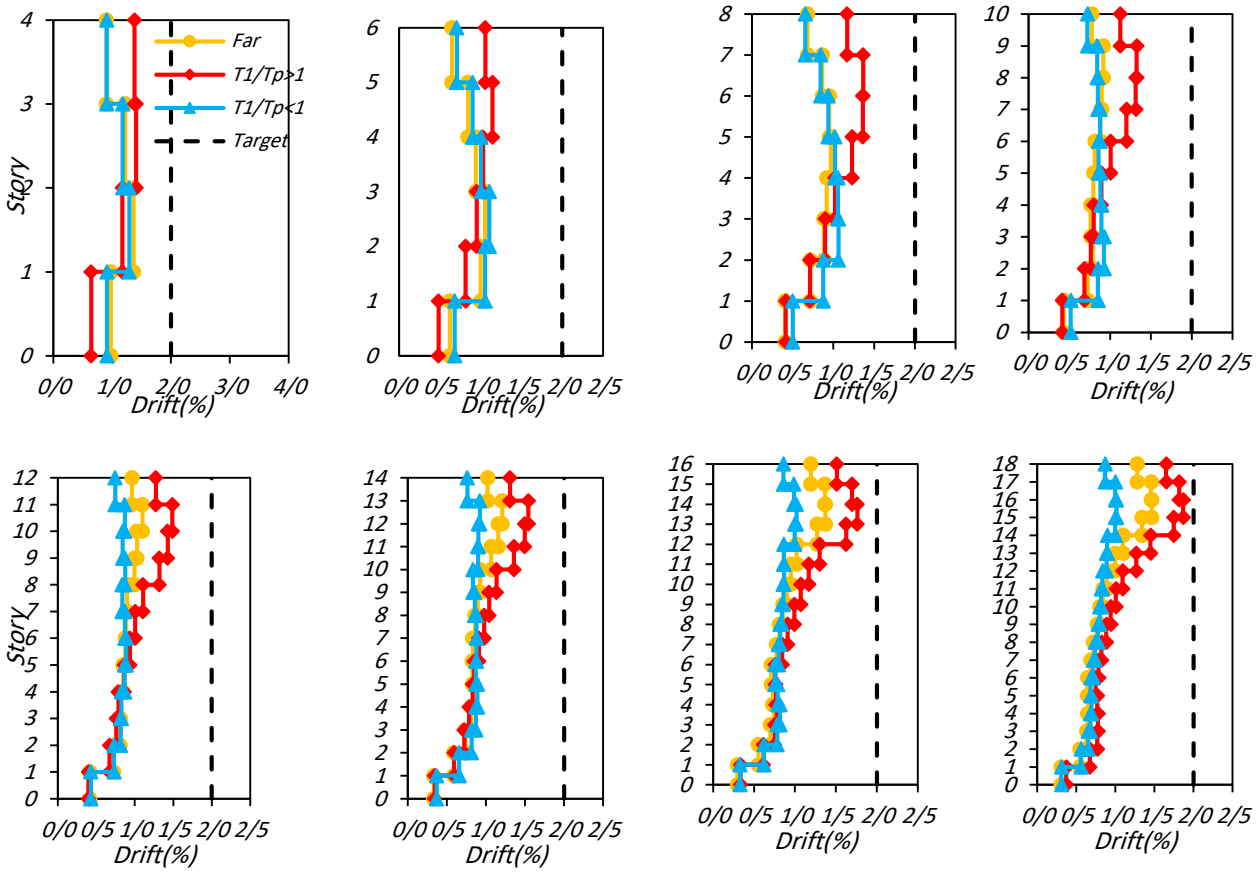

Figure. 7 Distribution of mean drifts over the height of structures subjected to far-fault, near-fault with $T_1/T_p \geq 1$ and near-fault with $T_1/T_p < 1$ records

The maximum values of the dispersion coefficient of drifts obtained from various structures across three record categories, namely far-fault, near-fault with $T_1/T_p \geq 1$, and near-fault with $T_1/T_p < 1$, are illustrated in Fig. 8. As anticipated, the near-fault records with $T_1/T_p \geq 1$ exhibits the highest dispersion coefficient. As previously mentioned, the drift values associated with this record category have the most significant impact on the upper stories of the structures, necessitating substantial displacement in these levels.

[DOI: 10.22068/ijoce.2024.14.1.574]

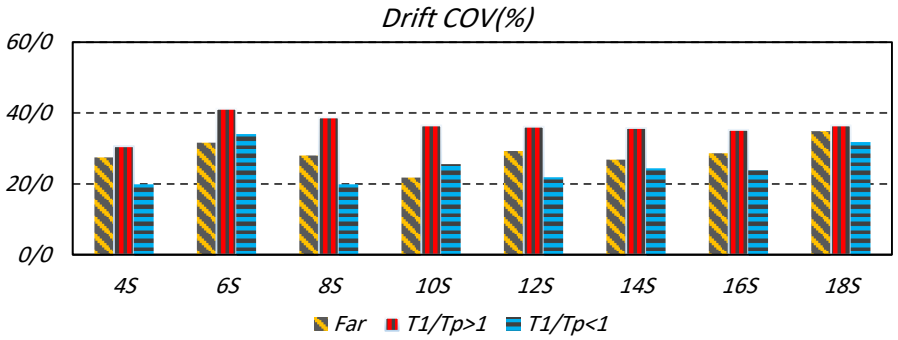

Figure 8. Effect of three categories records on the dispersion of the maximum drift demands

5.2. Relative distribution of the maximum story shear strength ratio

In this section, to more examine the effect of the ratio of fundamental period to ground motion pulse, the relative distribution of the maximum story shear strength ratio (V_i/V_n) is computed and the results are illustrated in Fig. 9 for the three selected record categories i.e., far-fault, near-fault with $T_1/T_p \geq 1$, and near-fault with $T_1/T_p < 1$.

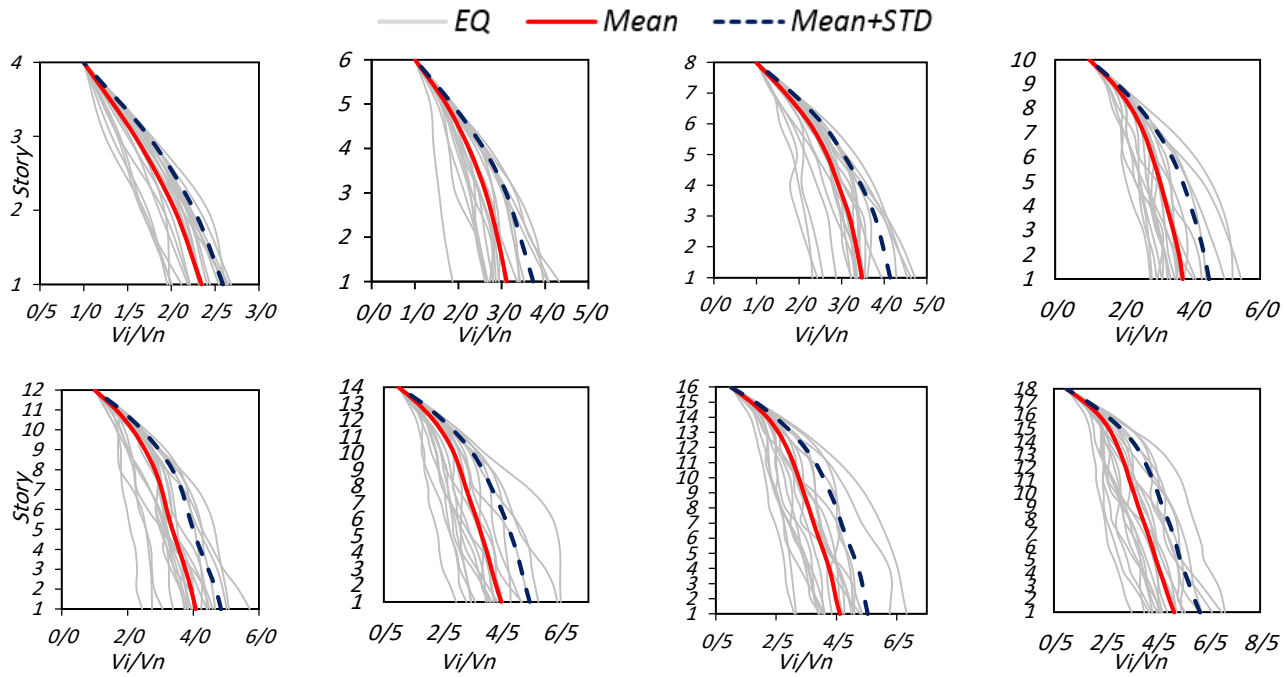

Figure. 9. (a) Comparison of Relative Shear Distributions under effect of far-fault records

[DOI: 10.22068/ijoce.2024.14.1.574]

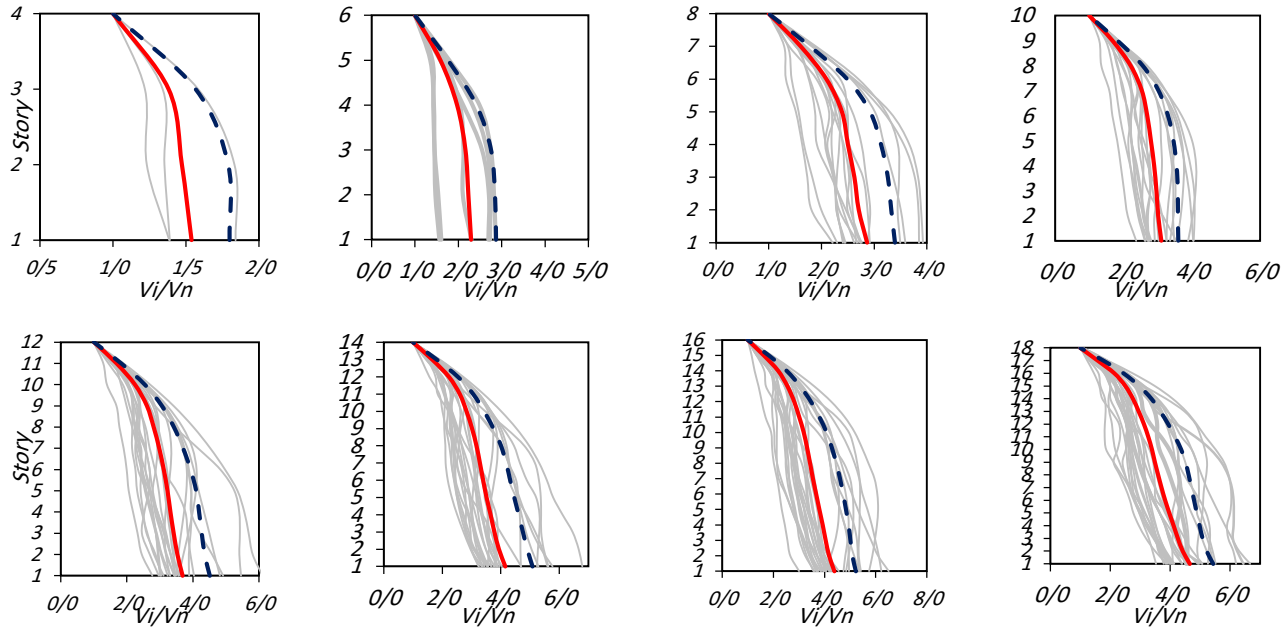

Figure. 9 (b) Comparison of Relative Shear Distributions under effect of near-fault records with $T_1/T_p \geq 1$

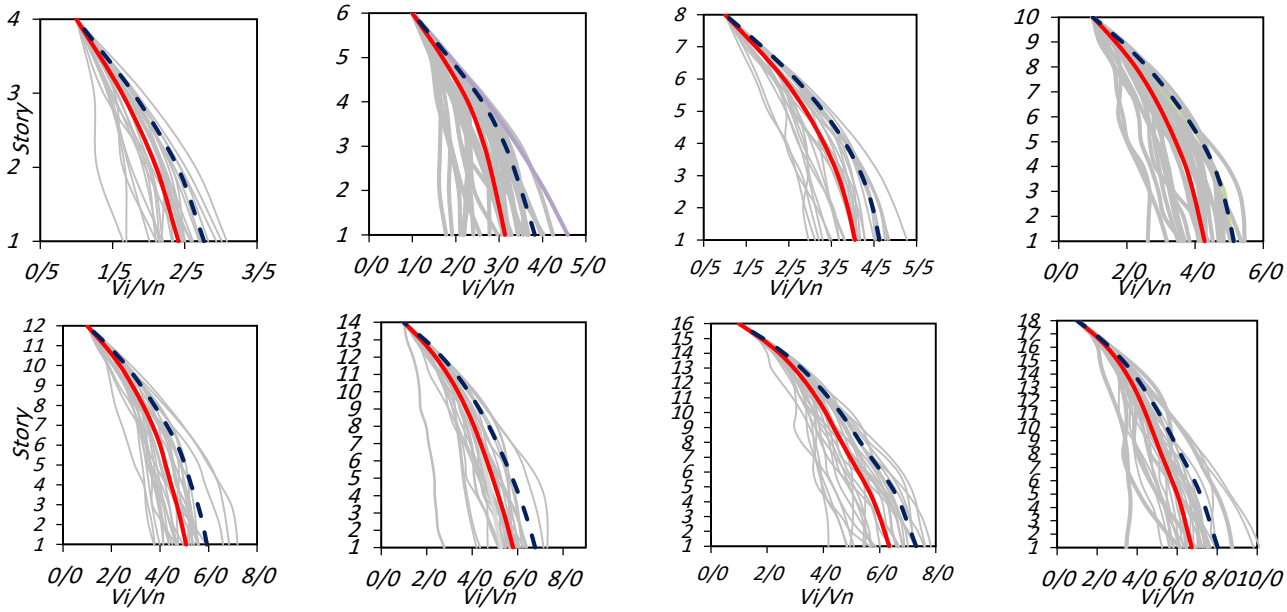

Figure. 9 (c) Comparison of Relative Shear Distributions under effect of near-fault records with $T_1/T_p < 1$

Additionally, Fig. 10 provides a comparison of this ratio across the three mentioned record categories. It is evident that the highest V_i/V_n ratio corresponds to the near-fault records with $T_1/T_p < 1$ category, and this ratio significantly increases with the number of stories within

[DOI: 10.22068/ijoce.2024.14.1.574]

this record category. In structures ranging from 4 to 18 stories, the V_i/V_n ratio in this category exceeds the corresponding ratio for the far-fault record category, ranging from 3% to 37% for different structures. This substantial increase highlights the distinct frequency content of the near-fault records with $T_1/T_p < 1$ category, which can impact the design process by imposing greater base shear strength on the structure.

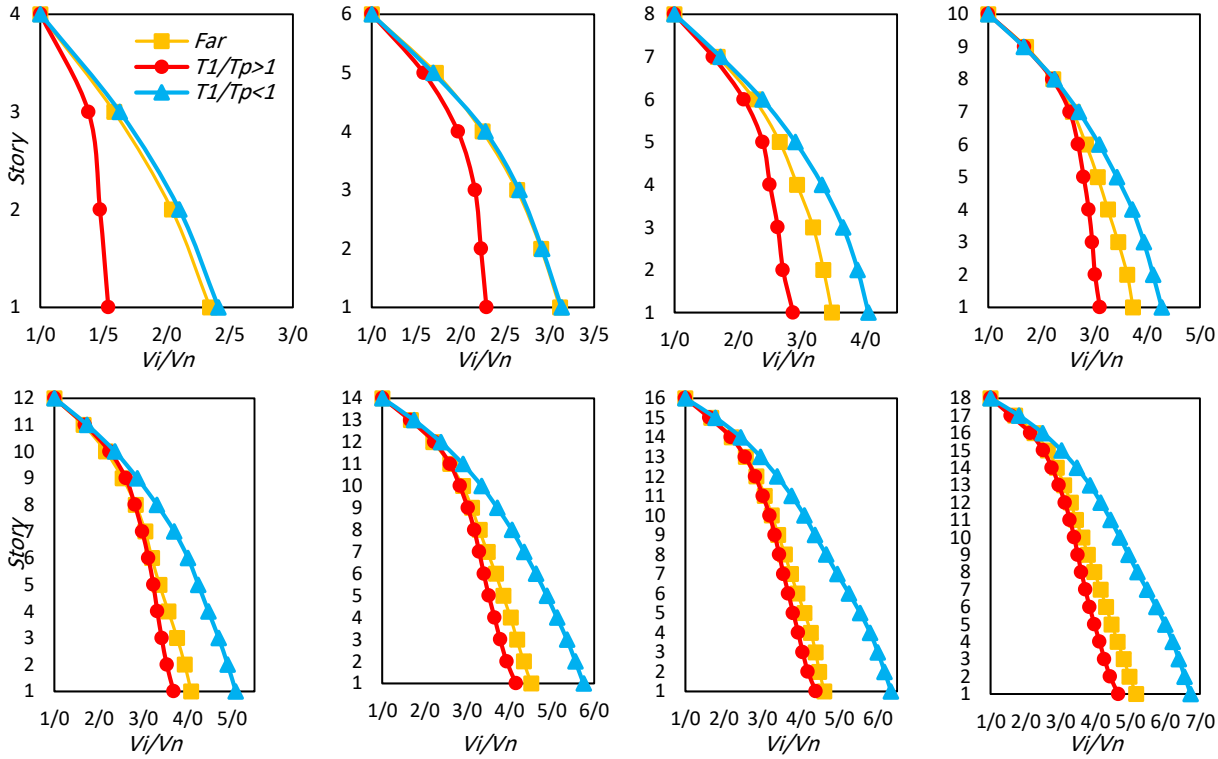

Figure. 10 Comparison of Relative Shear Distributions under effect of far-fault, near with $T_1/T_p \geq 1$ and near with $T_1/T_p < 1$

5.3. Optimizing Shear Strength Distribution Factor by Genetic Programming

Initially, a genetic programming (GP) approach is employed on the dataset. The training dataset is utilized to generate the models, which are subsequently evaluated using a separate testing dataset. The model that demonstrates a high coefficient of determination (R^2) for both the training and testing datasets is considered the robust model. The optimal model is achieved when employing a population size of 450 and conducting 100 generations. In this particular model, the best performance is achieved with minimal error. The predicted output values (y) are obtained by extracting data from the generated graphs of the GP models. Initially, based on the analysis of the time history of structures ranging from 4 to 18 stories, the data obtained were classified into two categories: far-fault records and near-fault records. For each category, separate test and training datasets were created. In previous studies, the relationship of variable "b" was determined using Eq. (8). However, in this research, an additional variable is

[DOI: 10.22068/ijoce.2024.14.1.574]

considered, which is the height of the structures. This variable, in addition to the structure's period, plays a key role in determining the base shear for design purposes. To enhance correlation, the data from the two categories of near-fault records are merged into a single group. This unification allows for a more comprehensive analysis and improves the overall correlation between the variables. The formula generated by the GP model for near-fault records is presented as Eq. (15). It is important to note that this formula holds true universally. The overall GP expression has been simplified for convenience:

$$b = 10.4T_1 - 0.0142H - 6.65\sin(T_1) + 0.0122T_1H - 3.58H_1^2 - 0.234 \quad (15)$$

To evaluate the efficiency of the models, the predicted values from the training dataset were compared with the testing dataset. Generally, the R^2 value obtained from the testing dataset is lower than that of the training dataset. The robust model is identified as the one where the testing R^2 value closely approximates the training R^2 value. The training and testing performances of the robust GP models for near-fault records are depicted in Fig.11.

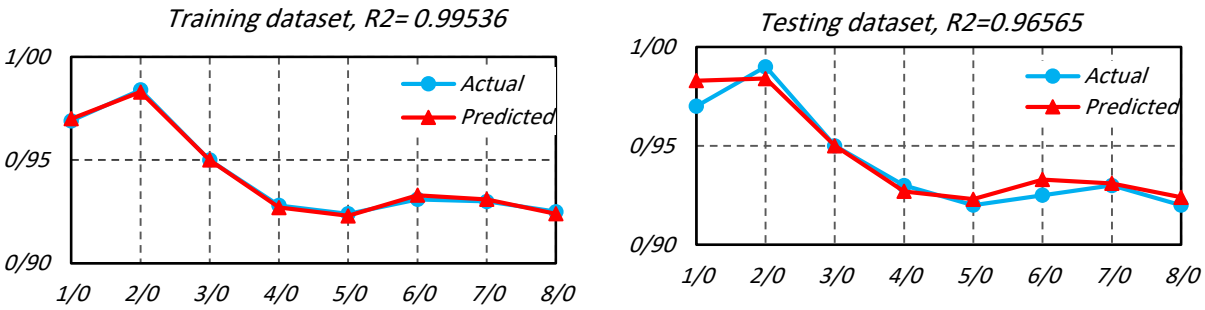

Figure 11. Performance of training and testing dataset for GP – Near-fault records

The Eq. (15) provides the most accurate relationship between the input variables and the expected output, minimizing the error. The performance of the model on both the training and testing datasets, along with the corresponding R values, is illustrated in Fig. 11. This figure provides a visual representation of the model's performance and its ability to fit the data accurately.

[DOI: 10.22068/ijoce.2024.14.1.574]

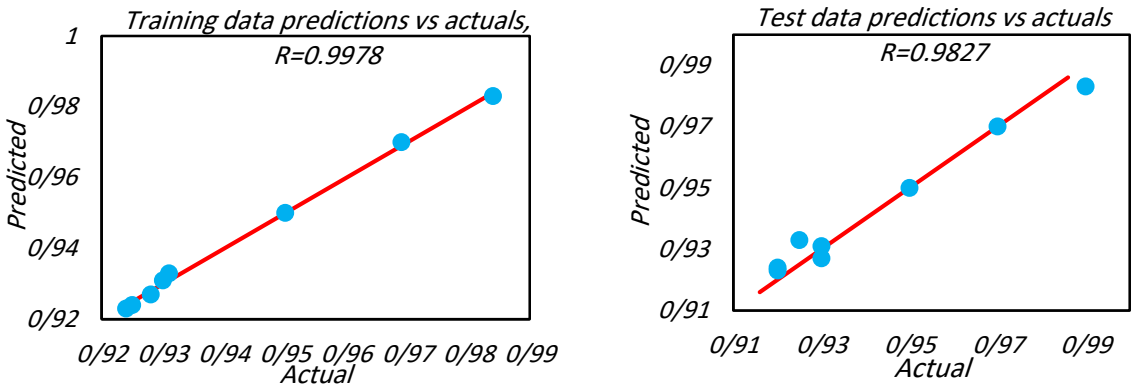

Figure 12. Performance of training and testing dataset for b – Near-fault records

Eq. (16) represents the relationship for variable "b" in the case of far-fault records. It is important to note that the two terms in this equation have coefficients that are very small. Therefore, these terms can be neglected, resulting in a simplified approximation of the equation, as shown in Eq. (17). This approximation provides a good estimation while reducing the complexity of the equation.

$$b = 0.0261H - 0.518T_1 - 0.0157T_1H + 0.129T_1^2 + 7.96\times10^{-5}T_1H^2 + 7.96\times10^{-5}T_1^2H + 1.04 \quad (15)$$

$$b = 0.0261H - 0.518T_1 - 0.0157T_1H + 0.129T_1^2 + 1.04 \quad (16)$$

The training and testing performances of the robust GP models for far-fault records are depicted in Figure 13.

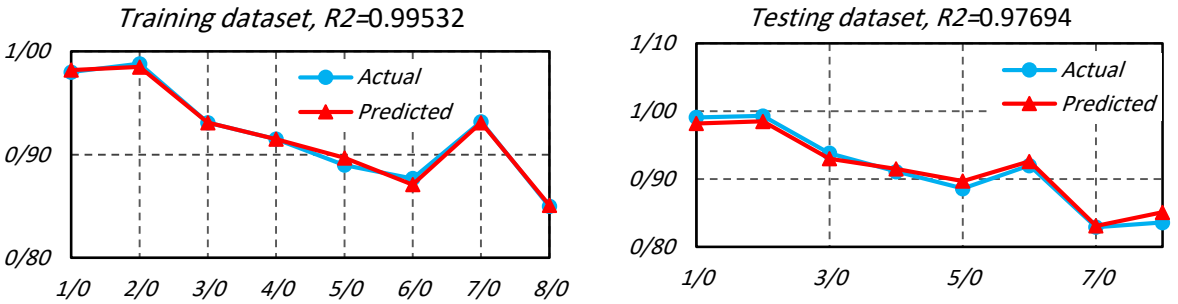

Figure 13. Performance of training and testing dataset for GP – Far-fault records

The performance of the model on both the training and testing datasets, along with the corresponding R values, for far-fault records is illustrated in Figure 14.

[DOI: 10.22068/ijoce.2024.14.1.574]

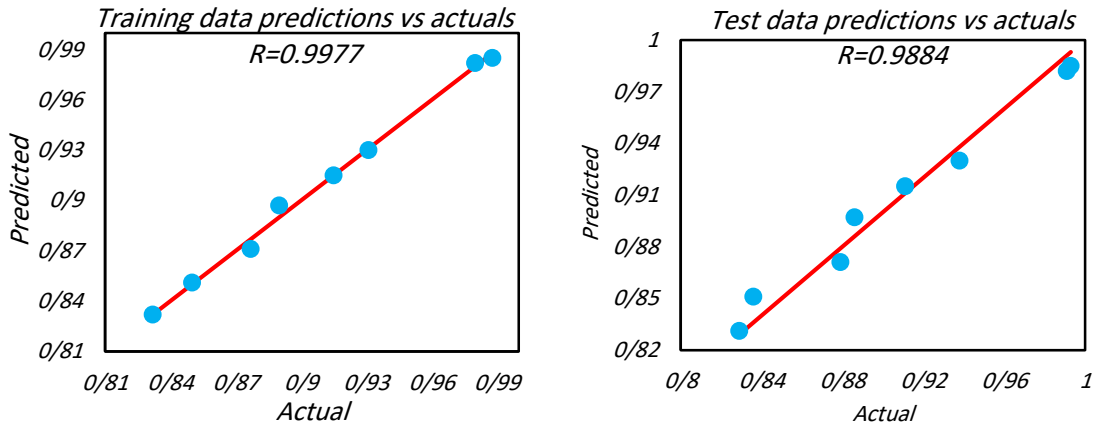

Figure 14. Performance of training and testing dataset for b – Far-fault records

7. CONCLUSION

This study provides a parametric investigation into the effects of far-fault and near-fault records on steel moment frames designed using the performance-based plastic design (PBPD) method. Eight frames designed with PBPD were subjected to both far-fault and near-fault conditions, specifically categorized as $T_1/T_p \geq 1$ and $T_1/T_p < 1$. In this regard, a large number of 90 near-fault and 22 far-fault strong ground motions are compiled and considered for nonlinear dynamic analyses. The findings reveal notable distinctions in the behavior of frames exposed to near-fault and far-fault records. Frames subjected to near-fault records with the $T_1/T_p \geq 1$ category exhibit significantly higher maximum drifts in the upper stories. The maximum drifts for frames ranging from 4 to 18 stories vary from 28.4% to 71.1%, indicating the increased vulnerability of these structures. Conversely, near-fault records with the $T_1/T_p < 1$category have a more pronounced impact on mid-rise frames compared to other categories. In structures with 4 and 6 stories, the maximum drift of the $T_1/T_p < 1$ records category is respectively 6.6% and 10% higher than that of the far-fault records category. However, as the frame height increases in structures with 8 and 10 stories, the $T_1/T_p < 1$ records category experiences the highest drift in the lower floors, with differences reaching 22.8% and 20.1% for these frames, respectively.

For practical purpose, to optimize the seismic parameters for design lateral force distribution (b), a robust model was developed using genetic programming, specifically GPTIPS. The genetic programming model, with a population size of 450 and 100 generations, achieved high coefficient of determination values. When tested with near-fault records, the training and testing models yielded coefficients of determination of 0.995 and 0.965, respectively. Similarly, for far-fault records, the corresponding values were 0.995 and 0.977. These results, regardless of the type of seismic records, demonstrate the effectiveness of the genetic programming model in accurately predicting and optimizing the seismic parameters for lateral force distribution in steel moment frames,.

[DOI: 10.22068/ijoce.2024.14.1.574]

REFERENCES

1. Leelataviwat S, Goel SC, Stojadinović B. Toward performance-based seismic design of structures, *Earthq. Spectra*, 1999; **15**: 435–461.
2. Lee S, Goel SC. *Performance-based design of steel moment frames using target drift and yield mechanism*, The University of Michigan, 2001.
3. Leelataviwat S, Goel SC, Stojadinović B. Energy-based seismic design of structures using yield mechanism and target drift, *J Struct Eng*, 2002; **128**(8): 1046–1054.
4. Bayat MR. *Performance-based plastic design of earthquake resistant steel structures: concentrically braced frames, tall moment frames, plate shear wall frames*, The University of Texas at Arlington, 2010.
5. Liao WC. *Performance-based plastic design of earthquake resistant reinforced concrete moment frames*, University of Michigan, 2010.
6. Liao WC, Goel SC. PBSD *of RC SMF using target drift and yield mechanism as performance criteria*, University of Michigan, 2010.
7. Karamodin A, Zanganeh A. Seismic design and performance of dual moment and eccentrically braced frame system using PBPD method, *Lat Am J Solids Struct*, 2017; **14**(3): 441–463.
8. Shayanfar MA, Rezaeian AR, Zanganeh A. Seismic performance of eccentrically braced frame with vertical link using PBPD method, *Struct Des Tall Spec Build*, 2012; **23**(1): 1-21.
9. Chao SH, Goel SC. Performance-based plastic design of special truss moment frames, *Eng J*, 2008; 45(2): 127.
10. Sahoo DR, Chao SH. Performance-based plastic design method for buckling-restrained braced frames, *Eng Struct*, 2010; **32**(9): 2950–2958.
11. Hung CC, Lu WT. A performance-based design method for coupled wall structures, *J Earth Eng*, 2017; **21**(4): 579–603.
12. Abdollahzadeh GR, Kuchakzadeh H, Mirzagoltabar A. Performance-based plastic design of moment frame-steel plate shear wall as a dual system, *Civil Eng Infrastruc J*, 2017; **50**(1): 21–34.
13. Bai J, Ou J. Earthquake-resistant design of buckling-restrained braced RC moment frames using performance-based plastic design method, *Eng Struct*, 2016; **107**: 66–79.
14. Ganjavi B, Gholamrezatabar A, Hajirasouliha I. Effects of soil-structure interaction and lateral design load pattern on performance-based plastic design of steel moment resisting frames, *Struct Des Tall Spec Build*, 2019; **28**(11): 1–15.
15. Rezaie F, Mortezaie H. Considering the soil effects on design process of performance-based plastic design for reinforced concrete structures, *Civil Eng Infrastruct J*, 2017; 50(2): 411–425.
16. Mortezaie H, Rezaie F. Optimization and evaluation of three-dimensional high-rise concrete structure equipped by TMD with considering the soil-structure interaction effect, *J V E*,2018; **20**(5): 2099–2110.
17. Abdollahzadeh G, Mohammadgholipour A, Omranian E. Seismic Evaluation of Steel Moment Frames Under Mainshock – Aftershock Sequence Designed by Elastic Design and PBPD Methods Seismic Evaluation of Steel Moment Frames Under Mainshock –

[DOI: 10.22068/ijoce.2024.14.1.574]

Aftershock Sequence Designed by Elastic Design and PBPD Methods, *J Earthq Eng*, 2018; **23**(10): 1605-1628.
18. Qiu CX, S. Zhu S. Performance-based seismic design of self-centering steel frames with SMA-based braces, *Eng Struct*, 2017; **130**: 67–82..
19. Hou H, Li H, Qiu C. Effect of hysteretic properties of SMAs on seismic behavior of self - centering concentrically braced frames, *Struct Control Health Monit*, 2017; **25**(3): 1–14.
20. Ganjavi B, Hadinejad A, Jafarieh AH. Evaluation of ground motion scaling methods on drift demands of energy-based plastic designed steel frames under near-fault pulse-type earthquakes, *Steel Compos Struct*, 2019; **32**(1): 91–110,.
21. Newmark NM, Hall WJ. *Earthquake spectra and design*, Berkeley, CA Earthq Eng Res Institute, Univ California, 1982.
22. Koza JR. Genetic Programming III - Darwinian Invention and Problem Solving, *Evol Comput*, 1999; **7**(4): 451–453.
23. Searson DP, Leahy DE, Willis MJ. GPTIPS: An Open Source Genetic Programming Toolbox For Multigene Symbolic Regression, *In Proceedings of the International multiconference of engineers and computer scientists*, 2010, Citeseer, pp. 77-80.
24. Kaveh A, Khalegi A. Prediction of strength for concrete specimens using artificial neural network, *Asian J Civ. Eng* , 2000; **2**(2): 1-13.
25. Searson DP. *GPTIPS 2: An Open-Source Software Platform for Symbolic Data Mining BT-Handbook of Genetic Programming Applications*, Springer International Publishing, 2015, pp. 551–573.
26. Baykasoğlu A, Güllü H, Çanakçı H, Özbakır L. Prediction of compressive and tensile strength of limestone via genetic programming, *Expert Syst Appl*, 2008; **35**(1): 111–123, 2008.
27. Savic DA, Walters GA, Davidson JW. A Genetic Programming Approach to Rainfall-Runoff Modelling, *Water Resour Manag*, 1999; **13**(3): 219–231.
28. Gandomi AH, Alavi AH. A new multi-gene genetic programming approach to non-linear system modeling. Part II: geotechnical and earthquake engineering problems, *Neural Comput Appl*, 2011; **21**: 189–201.
29. Gandomi AH, Alavi AH. A new multi-gene genetic programming approach to nonlinear system modeling. Part I: materials and structural engineering problems, *Neural Comput Appl*, 2011; **21**: 171–187.
30. Moradi M, Bagherieh AR, Esfahani MR. Damage and Plasticity Constants of Conventional and High-Strength Concrete Part Ii : Statistical Equation Development Using, *Int J Optim Civil Eng*, 2018; **8**(1), 77-99.
31. Kaveh A, Servati H. Neural Networks for the Approximate Analysis and Design of Double Layer Grids, *Int J Sp Struct*, 2002; **17**(1): 77–89.
32. Fattahi H, Ebrahimi Farsangi MA, Shojaee S, Nekooei K, Mansouri H. Application of the hybrid harmony search with support vector machine for identification and calssification of damaged zone around underground spaces, *Int J Optim Civil Eng*, 2013; **3**(2): 345-58
33. Kaveh A, Zakian P. Performance based optimal seismic design of rc shear walls incorporating soil–structure interaction using css algorithm," *Int J Optim Civil Eng*, 2012; **2**(3): 383–405.

[DOI: 10.22068/ijoce.2024.14.1.574]

34. Uang CM, Bertero VV. Evaluation of seismic energy in structures, *Earthq Eng Struct Dyn*, 1990; **19**(1): 77–90.
35. Chopra AK. *Dynamics of Structures*, Pearson Education India, 2013.
36. Chou C, Uang CM. A procedure for evaluating seismic energy demand of framed structures, *Earthq Eng Struct Dyn*, 2003; **32**(2): 229–244.
37. Housner GW. Limit design of structures to resist earthquakes, *In Proc. World Conference of Earthquake Engineering*, 1956.
38. Housner G. *Earthquake-resistant limit-state design for buildings*, University of Tokyo Press, 1985.
39. Goel SC, Liao WC, Reza Bayat M, Chao SH. Performance-based plastic design (PBPD) method for earthquake-resistant structures: an overview, *Struct Des Tall Spec Build*, 2010; **19**(1): 115–137.
40. Chao SH, Goel SC, Lee SS. A seismic design lateral force distribution based on inelastic state of structures," *Earthq Spectra*, 2007; **23**: 547–569.
41. Goel SC, Liao WC, Bayat MR, Chao SH. Performance-based plastic design (PBPD) method for earthquake-resistant structures: An overview, Struct Des Tall Spec Build, 2010; **19**(1–2),:115–137.
42. McKenna GL, Scott F, Fenves MH. *PEER, Open System for Earthquake Engineering Simulation (OpenSees) Ed*. University of California, Berkeley: Pacific Earthquake Engineering Research Center; 2017.
43. Alavi B, Krawinkler H. *Effects of near fault ground motions on frame structures*, Stanford: John A. Blume Earthquake Engineering Center, 2001.
44. Baker JW, Lin T, Shahi SK, Jayaram N. *New ground motion selection procedures and selected motions for the PEER transportation research program*, PEER report 3, 2011.
45. *NEHRP Recommended seismic provisions for new buildings and other structures*, Building Seismic Safety Council, 2001.
46. U. S. G. Survey, USGS Website: https://earthquake.usgs.gov/hazards/hazmaps/, 2020.

[DOI: 10.22068/ijoce.2024.14.1.574]